

• Original Paper •

Sensitivity to Tendency Perturbations of Tropical Cyclone Short-range Intensity Forecasts Generated by WRF

Xiaohao QIN, Wansuo DUAN*, and Hui XU

*State Key Laboratory of Numerical Modeling for Atmospheric Sciences and Geophysical Fluid Dynamics,
Institute of Atmospheric Physics, Chinese Academy of Sciences, Beijing 100029, China*

(Received 6 September 2019; revised 8 November 2019; accepted 19 November 2019)

ABSTRACT

The present study uses the nonlinear singular vector (NFSV) approach to identify the optimally-growing tendency perturbations of the Weather Research and Forecasting (WRF) model for tropical cyclone (TC) intensity forecasts. For nine selected TC cases, the NFSV-tendency perturbations of the WRF model, including components of potential temperature and/or moisture, are calculated when TC intensities are forecasted with a 24-hour lead time, and their respective potential temperature components are demonstrated to have more impact on the TC intensity forecasts. The perturbations coherently show barotropic structure around the central location of the TCs at the 24-hour lead time, and their dominant energies concentrate in the middle layers of the atmosphere. Moreover, such structures do not depend on TC intensities and subsequent development of the TC. The NFSV-tendency perturbations may indicate that the model uncertainty that is represented by tendency perturbations but associated with the inner-core of TCs, makes larger contributions to the TC intensity forecast uncertainty. Further analysis shows that the TC intensity forecast skill could be greatly improved as preferentially superimposing an appropriate tendency perturbation associated with the sensitivity of NFSVs to correct the model, even if using a WRF with coarse resolution.

Key words: sensitivity, tendency perturbation, tropical cyclone, intensity, forecasts

Citation: Qin, X. H., W. S. Duan, and H. Xu, 2020: Sensitivity to tendency perturbations of tropical cyclone short-range intensity forecasts generated by WRF. *Adv. Atmos. Sci.*, **37**(3), 291–306, <https://doi.org/10.1007/s00376-019-9187-6>.

Article Highlights:

- Model error is an important source of TC short-range intensity forecast error.
- The model errors associated with the potential temperature in the inner core and middle layers of the atmosphere of TCs influence the TC intensity forecast skill.

1. Introduction

As a common type of severe weather event, tropical cyclones (TCs) are a double-edged sword. TC rainfall can greatly relieve high temperatures and droughts, but they can also cause disruption to human activities, economic losses, and even human fatalities. TCs attract the attention of both the general public and scientists worldwide, and an accurate forecast for TCs is of special concern. The forecast of TCs can not only help decision makers issue alarms as soon as possible and provide information to the general public for arranging their necessary production and life activities, but can also help the government take measures to reduce economic and human losses caused by TCs.

The short-range forecast skill (with one- to two-day

lead times) of TC intensity is far behind that of the TC track (DeMaria et al., 2014) and less improved than the longer lead times' forecast skill during the recent 30 years. However, these one-to-two days are critical with respect to TCs because nearly all protective measures are carried out within this period. Therefore, it is necessary to reduce the forecast uncertainty of TC intensity, even with short lead times; a feasible and effective way is to identify the sources that contribute to forecast uncertainty and then reduce the uncertainties accordingly. It is known that inaccurate initial conditions and imperfect numerical models are two main sources for forecast uncertainty. For the former, many studies have diagnosed their impacts on TC intensity forecasts. For example, Torn (2016) found that the initial uncertainty associated with the atmosphere produces the largest standard deviation in TC intensity forecasts, and the initial uncertainty associated with the oceans leads to continuous growth in ensemble standard deviation with time development.

* Corresponding author: Wansuo DUAN
Email: duanws@lasg.iap.ac.cn

Emanuel and Zhang (2016) found that the error growth associated with TC intensity over the first few days is dominated by the errors in initial intensity of TCs in terms of the perfect model scenario; they particularly thought that the growth of TC intensity forecast errors are at least as sensitive to the specification of inner-core moisture as to that of the wind field (Emanuel and Zhang, 2017).

Forecast errors can also be produced due to model imperfections. For TC intensity forecasts, Emanuel and Zhang (2016) emphasized that the errors in initial TC intensity are an important source of forecast error. However, there was still a large root-mean-square error gap between the real-time operational model forecast and their perfect model predictability experiments, which indicates that model error plays an important role. Many factors contribute to model errors, such as incomplete knowledge of a physical process and its ancillary data, reduced complexity to limit computational costs, omission or misrepresentations of processes and system components, uncertain parameters in parameterizations that do not have a directly observable equivalent, discretization, and insufficiently fine resolution (Leutbecher et al., 2017). For example, considering uncertain parameters, Green and Zhang (2013) examined the effect of surface fluxes on the intensity and structure of TCs using the convection-permitting Weather Research and Forecasting (WRF) model. They found that the drag coefficient affects the pressure–wind relationship and changes the radius of the maximum near-surface winds of a storm. By contrast, Torn (2016) found that the uncertainty in drag coefficient led to negligible increases in the standard deviation of TC intensity forecasts, which is mainly due to the lack of spatial correlation in the exchange coefficient perturbations. In addition, some studies emphasized that increasing spatial resolution can help resolve various scales of motion and improve the forecast of TC intensity, whereas model convergence does not occur, even with grid spacing well below 1 km (Gentry and Lackmann, 2010).

How to describe model uncertainties in numerical predictions is a challenging problem due to their complexity. Two main approaches have been used to represent model uncertainties: one uses multi-model or multi-parameterization, and the other uses stochastic representation. For the former, Bhattia et al. (2017) used two statistical and two dynamic models and proposed the prediction of intensity model error (PRIME) forecasting scheme. They found that the PRIME error forecasts were significantly better than the forecasts that used error climatology derived from a majority of historical forecasts for a majority of forecast hours, and the bias-corrected forecasts using PRIME had significantly lower errors than the original forecasts. However, the sampling of uncertainty in this way is discrete and the increase of the spread is simply due to different model biases and cannot provide a reasonable distribution of ensemble members. There are three main approaches for the stochastic representation of model uncertainties: the stochastically perturbed parametrization tendency scheme (SPPT: Buizza et al., 1999; Palmer et al., 2009), the stochastic kinetic energy backscatter scheme

(SKEB: Berner et al., 2009; Judt et al., 2016), and the stochastically perturbed parameterization scheme (SPP: Ollinaho et al., 2017). The SPPT scheme assumes that the dominant error of the parameterized physics is proportional to the net physics tendency. SPPT has been found to be effective in generating additional ensemble spread and improving probabilistic skill in a range of numerical model prediction ensembles (Leutbecher et al. 2017). In TC forecasts, Puri et al. (2001) showed that SPPT strongly influences the central pressure of the TC but has less effect on the TC track. The SKEB scheme aims to represent model uncertainties associated with scale interactions that take place in the real atmosphere but are absent in a truncated numerical model. Reynolds et al. (2011) demonstrated that SKEB increases the ensemble spread, especially in the tropics. However, Leutbecher et al. (2017) showed that SKEB adds little additional spread for different lead-time forecasts. In Lang et al. (2012), they compared SPPT with SKEB and found that their perturbation structures are initially quite different but after two days they converge toward a TC displacement and take shape in an intensity-change pattern. Lang et al. (2012) also compared the SPP scheme with SPPT and found that the former is more flexible and introduces local stochastic perturbations to both parameters and variables in the parameterizations. Moreover, SPP was also found to be more effective than SPPT in generating ensemble spread in TC intensity forecasts. It is clear that the approaches mentioned above behave differently in generating ensemble spread when either the forecast time (short- and medium-range) or the target region (tropics or subtropics) changes. A possible reason is that those approaches do not sufficiently consider the unstable growth of model errors and make the increase of the ensemble spread case-, target-region-, and even model-dependent.

Against the stochastic representation of model uncertainty, Barkmeijer et al. (2003) proposed the forcing singular vector (FSV) concept, which is invariant during forecast periods and has a particular pattern and represents the constant tendency perturbation that has the fastest growth. They attempted to reveal the most disturbing tendency perturbations of the model, i.e., those that tend to yield aggressively large prediction departures. However, the FSV is established based on a linearized model and cannot fully reflect the effect of nonlinearity on model errors. Realizing this limitation of FSV, Duan and Zhou (2013) extended FSV to a nonlinear field and proposed the nonlinear forcing singular vector (NFSV) approach. The competing aspect of NFSV considers the effect of nonlinearity that exists in numerical models and is thus more applicable in describing the most disturbing tendency perturbation in predictability studies associated with model uncertainty. Since NFSV induces the largest perturbation growth, it has the most possibilities to increase the ensemble spread when it is used for ensemble forecasts generated by an unstable dynamical system and can overcome the limitation of the aforementioned approaches (Huo, 2016). Focusing on TC intensity, NFSV may depict the model perturbation that affects the TC intensity forecast

uncertainties at its greatest extent. It has been deduced that if such model perturbation is extracted from one control forecast, it may reveal the sensitivity to model errors of the control forecast of TC intensity. Using this sensitivity, one can determine where the TC intensity forecasting uncertainties are most sensitive to the model errors and propose the strategy of correcting the control forecast and improve the forecast skill for TC intensity. Therefore, for a weather forecast model we naturally ask: which features of the NFSV-tendency perturbation are associated with the TC intensity forecast, how do they influence the TC intensity forecast uncertainties, and how can we improve the TC intensity forecast skill using the sensitivity revealed by the NFSV-tendency perturbation?

In the present study, we attempt to adopt the WRF model to address the above questions. The rest of this paper is organized as follows. Section 2 briefly describes the NFSV approach. Section 3 introduces the WRF model and TC cases used in the present study. The structure of the NFSV-tendency perturbation is explored in section 4, and its impact on TC intensity and destructive force is illustrated in section 5. Section 6 presents interpretation of how NFSV-tendency errors affect TC intensity and the availability of utilizing the sensitivity of NFSVs to reduce the model uncertainty. Finally, section 7 provides a summary and discussion.

2. Nonlinear forcing singular vector

Suppose that a state variable U is predicted and its control forecast is governed by the equation $\partial U/\partial t = F(U(x; t))$, where $F(\cdot)$ is a nonlinear function. An external forcing f is superimposed on the right-hand side of the equation and a perturbation forecast can be obtained. The difference between control and perturbed forecasts can reveal the sensitivity of the control forecast to the model uncertainty described by the tendency perturbation f . If U is related to TC intensity, the above tendency perturbation f will ultimately lead to a large deviation from the control forecast in TC intensity. In the present study, we use the minimum sea level pressure (SLP) to depict the TC intensity, where SLP is calculated by Eq. (1):

$$SLP = P_{sfc} e^{\frac{2GZ_0}{R_d(SST+T_{sfc})}}, \tag{1}$$

where P_{sfc} and T_{sfc} denote the pressure and air temperature at the surface, Z_0 represents half the height of the lowest model vertical level, SST is the sea surface temperature, and the constants $G = 9.81 \text{ N kg}^{-1}$ and $R_d = 287.04 \text{ J kg}^{-1} \text{ K}^{-1}$ are gravitational acceleration and dry air gas constant..

A cost function with respect to the SLP is constructed as in Eq. (2) to describe the effects of the tendency perturbation f on TC intensity forecast uncertainty:

$$J(f) = \frac{1}{2} [SLP_{t=T}(x_0, f) - SLP_{t=T}(x_0, 0)]^2, \tag{2}$$

where $SLP_{t=T}(x_0, f)$ and $SLP_{t=T}(x_0, 0)$ respectively denote

the forecasted SLP at time T starting from the initial conditions x_0 with and without the tendency perturbation f (here, the latter, $SLP_{t=T}(x_0, 0)$, is just the SLP in the control forecast). The aforementioned NFSV (f^*) can be obtained by maximizing Eq. (2) when f is constrained to have a certain energy E . Therefore, it is known that the NFSV-type tendency perturbation represents the one that has the potential for yielding an aggressively large deviation of the SLP from the control forecast and has the largest effect on the TC intensity forecast, i.e., the TC intensity in the control forecast is most sensitive to the NFSV-tendency perturbation. Consequently, the NFSV-tendency perturbation can tell us which state variable in which region in the control forecast should be preferentially corrected to reduce the uncertainty of control forecasts or should be preferentially tendency-perturbed to effectively increase the ensemble spread to improve the ensemble forecast skill for TC intensity.

The NFSV approach has been applied to identify the most disturbing tendency error of the Zebiak–Cane model associated with El Niño predictions (Duan and Zhao, 2015). Duan et al. (2014), according to the NFSV tendency perturbation structure, corrected the model errors of the Zebiak–Cane model by assimilating the tendency perturbation and reproduced the diversities of ENSO that most models fail to reproduce. It is clear that the NFSV is an effective approach that provides useful information for correcting the model. It is expected here that the NFSV can also identify the sensitive model uncertainty most likely to influence the TC intensity forecast and improve its forecast skill.

We use optimization algorithms to calculate the NFSV associated with the TC intensity forecast. However, the existing optimization solvers are often used to solve minimization problems. The NFSV is related to a maximization problem. Therefore, for the NFSV, we must reverse the NFSV-related maximization problem of Eq. (2) into a minimization one by taking the negative of Eq. (2), $J_1(f) = -J(f)$, and then use the existing optimization solvers to calculate it. In the present study, we adopt the “spectral projected gradient 2” solver (SPG2; Birgin et al., 2001) to calculate the NFSV of the control forecasts of TC intensity. In terms of the TC intensity of concern in Eq. (1), the tendency perturbations are considered to be superimposed on the tendency of potential temperature and/or moisture to calculate the NFSV of the control forecast. Although horizontal winds are also important for depicting the TC intensity, it does not appear in Eq. (1) for the TC intensity and is thus not used to calculate the NFSV. The calculated NFSV-tendency perturbations are correspondingly referred to as “NFSV-T” for potential temperature, “NFSV-Q” for moisture, and “NFSV-TQ” for their combined mode. Moreover, to ensure the feasibility of the magnitude of the tendency perturbations, the total energy (Zou et al., 1997; Ehrendorfer et al., 1999) of the tendency perturbations is constrained to be less than 0.05 J kg^{-1} , which is either not too small to have obvious impacts on the TC intensity or too large to make the model integration terminate. The total energy E is estimated as in Eq. (3):

$$E = \iiint_{\sigma,xy} \frac{1}{2} \left[\left(\frac{G}{N\theta} \right)^2 \theta'^2 + \frac{L^2}{C_p T_r} q'^2 \right] dy dx d\sigma. \quad (3)$$

The perturbation energy here is contributed by both tendency perturbation from potential temperature θ' and moisture q' in horizontal directions x and y and vertical direction σ , $L = 2.5104 \times 10^6 \text{ J kg}^{-1}$, $C_p = 1005.7 \text{ J kg}^{-1}$, $T_r = 270 \text{ K}$, and N is the Brunt–Vaisala frequency.

3. Model and TC cases

Version 3.6 of WRF and its adjoint model are used, with the initial fields and boundary conditions derived from ERA-Interim data at a resolution of $0.25^\circ \times 0.25^\circ$. Experiments are set up in one single domain of 29×29 grid points, with grid spacing of 90 km. In addition, 31 eta levels are adopted in the vertical direction, and the parameterization schemes are microphysical (Iscondscheme), planetary boundary layer (surfdrgascheme), and cumulus convective (ducuscheme). These schemes are utilized because their respective adjoint schemes are available for calculating the NFSV-type tendency perturbation. We first compare the TC simulations under different horizontal resolutions; the results are illustrated in Fig. 1. It is shown that the simulated minimum SLPs under different resolutions are almost the same in

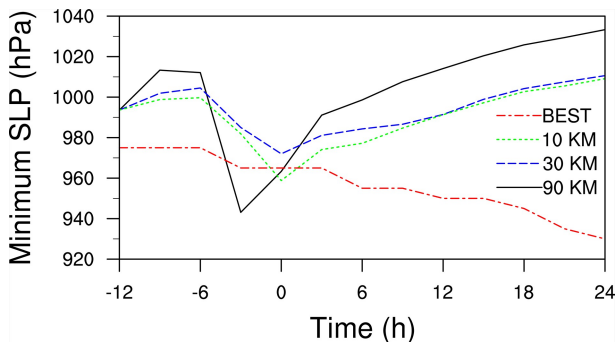


Fig. 1. Simulated minimum SLP at horizontal resolutions of 90 km (black), 30 km (blue), and 10 km (green) for the TC case Dujuan. The simulation is generated by the WRF model and the best-track data (red) are from the CMA.

experiencing a rapid drop within the first several hours and then gradually increasing, but all of them depart from the best track of the China Meteorological Administration (CMA). For different resolutions, the simulated minimum SLPs drop by approximately 20 hPa at the 24-h lead time, with the resolutions decreasing from 90 km to 30 km, whereas trivial differences occur in the minimum SLPs of TCs when the resolutions are further decreased from 30 km to 10 km. Obviously, the simulated minimum SLPs are sensitive to resolution. In the present study, the optimization algorithm used to calculate NFSV-tendency perturbation requires the sensitivity of model output to tendency perturbations, which is provided by the adjoint model, and the adjoint model is coded strictly according to the tangent linear model. However, the validity of the tangent linear model is verified to be much more acceptable when a 90-km horizontal resolution is used. Therefore, we have to use the WRF model with a 90-km horizontal resolution. Although the 90-km resolution is coarse and induces additional model errors with respect to the TC intensity forecast, it provides an opportunity for the sensitivities of NFSVs to demonstrate their applicability in reducing model errors. That is, it is investigated in the present study whether the ability to simulate TC intensity can be greatly improved using the sensitivity of the NFSVs even though the horizontal resolution of WRF is relatively coarse.

There are nine TC cases for investigation, all of which originated over the western North Pacific. Their basic information is detailed in Table 1. Among these TCs, three cases [i.e., Dujuan (2015), Parma (2009), and Meranti (2016)] experienced rapid intensification within 24 h, i.e., their near-surface maximum wind speed (MWS) increases by more than 15 m s^{-1} during this period. Another three cases [i.e., Fungwong (2014), Megi (2010), and Tembin (2012)] underwent obvious weakening during the 24 h, and the remaining three cases [i.e., Neoguri (2014), Nanmadol (2011), and Jangmi (2008)] maintained their intensity and had no obvious variation during this period. For all these nine cases, the model simulates much weaker storms than in reality, with a higher average minimum SLP of 82.5 hPa at a lead time of 24 h.

Table 1. Nine TC cases used in this study.

Name	Start time (0 h; UTC)	End time (24 h; UTC)	Intensity at start time	Intensity at end time
Dujuan (201521)	0000 26 Sep	0000 27 Sep	965 hPa/38 m s^{-1}	930 hPa/55 m s^{-1}
Parma (200917)	1200 29 Sep	1200 30 Sep	994 hPa/20 m s^{-1}	970 hPa/35 m s^{-1}
Meranti (201614)	0000 12 Sep	0000 13 Sep	955 hPa/42 m s^{-1}	910 hPa/65 m s^{-1}
Neoguri (201408)	0000 8 Jul	0000 9 Jul	935 hPa/52 m s^{-1}	966 hPa/38 m s^{-1}
Nanmadol (201111)	1200 26 Aug	1200 27 Aug	920 hPa/60 m s^{-1}	945 hPa/42 m s^{-1}
Jangmi (200815)	0000 29 Sep	0000 30 Sep	970 hPa/35 m s^{-1}	990 hPa/23 m s^{-1}
Fungwong (201416)	0000 21 Sep	0000 22 Sep	982 hPa/28 m s^{-1}	985 hPa/25 m s^{-1}
Megi (201013)	0000 20 Oct	0000 21 Oct	940 hPa/52 m s^{-1}	940 hPa/52 m s^{-1}
Tembin (201214)	0000 26 Aug	0000 27 Aug	965 hPa/38 m s^{-1}	975 hPa/33 m s^{-1}

Note: The numbers (No.) and intensities are from the best-track data of the CMA, the latter of which include the minimum SLP and maximum surface wind speed at the corresponding time.

4. NFSV Structure

For each case, we use a 12-h (from -12 h to 0 h) integration for spin-up. Then, starting from 0 h, we integrate the WRF model for 24 h and use the SPG2 solver to calculate the NFSV-Ts, NFSV-Qs, and NFSV-TQs that are superimposed on the tendency of potential temperature, moisture, and both temperature and moisture, respectively. These NFSV-tendency perturbations represent the ones that lead to the largest deviation of the SLP from the control forecast at the 24-h lead time.

The NFSV-Ts of all nine cases are illustrated to have a

coherent barotropic structure with height and to be highly concentrated around the center of the TC at the 24-h lead time. The structure of the NFSV-T is independent of the actual intensities of the TC cases and what they will experience in the following 24 h and is only related to the final locations of the TCs at the 24-h lead time. This result implies that the track affects the forecast skill of intensity to some degree, which is in accordance with that in [Sippel and Zhang \(2010\)](#). That is, NFSV-T is related to the location of the TC at the time of concern (24 h here). As an example, we plot the NFSV-T for the TC case Dujuan in [Fig. 2](#). It is shown that the NFSV-T displays positive anomalies in the vertical

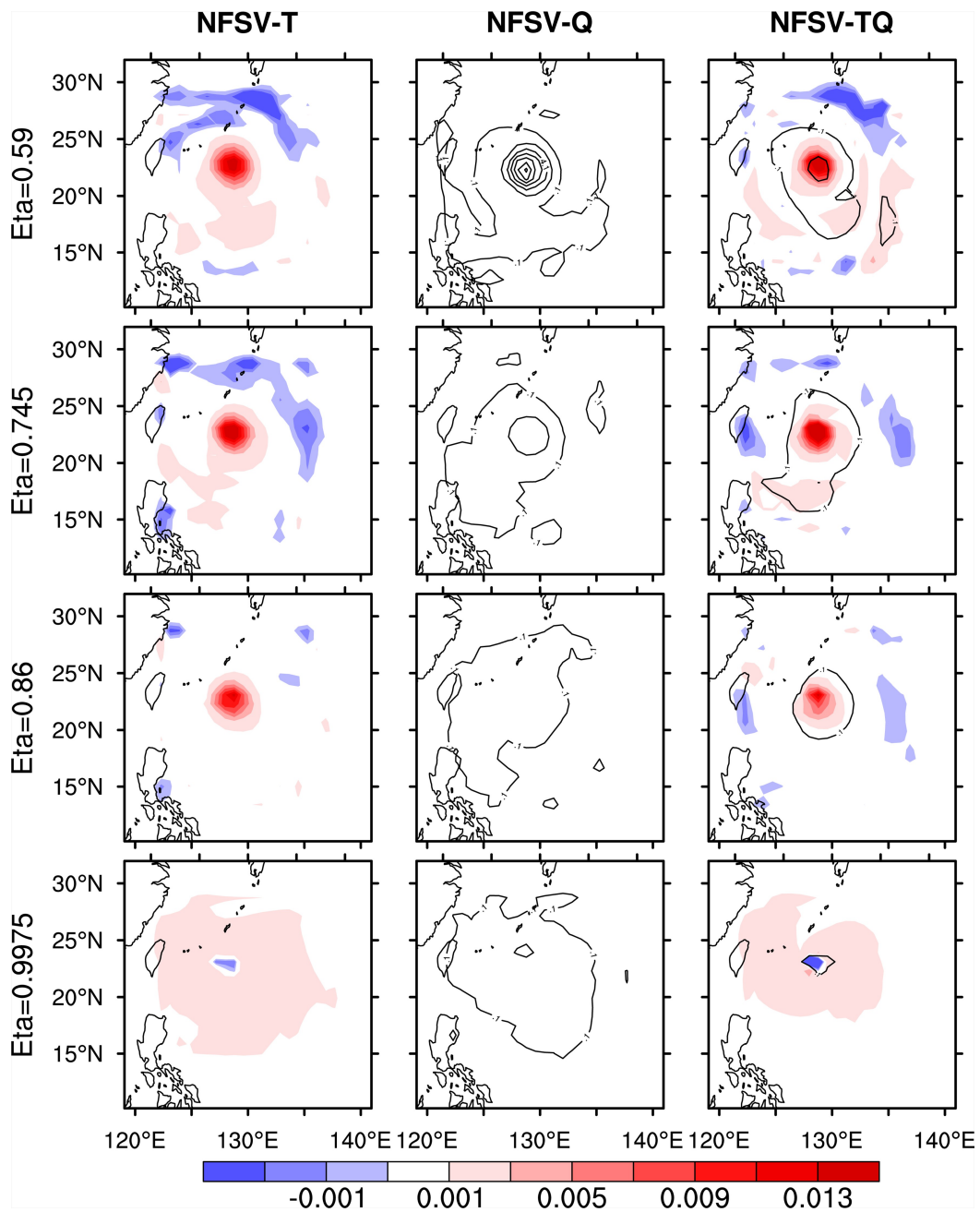


Fig. 2. The NFSV-T (left; units: $K s^{-1}$), NFSV-Q (middle; units: $kg kg^{-1} s^{-1}$), and NFSV-TQ [right; shading is for potential temperature (units: $K s^{-1}$), and contours are for moisture (unit: $kg kg^{-1} s^{-1}$)] for the TC case Dujuan at different eta levels.

layers, except for the surface layer, and is located around the center of the TC at the 24-h lead time; moreover, such anomalies are enhanced with height and reach the maximum at middle levels of the atmosphere (i.e., the level with eta = 0.59 in Fig. 2). Such NFSV-Ts indicate that the change of potential temperature anomalies superimposed at the position where the storm will move to at 24 h, compared with other locations, is more likely to influence the SLP and have the potential for yielding aggressively large deviation from the control forecast. In addition, in Fig. 3 we plot the inertial energy of the NFSV-T for the TC case Dujuan as a function of height, where the energy at each height is averaged over the region covered by the leading 49 grid points with the largest values of NFSV-Ts. It can be seen that the energies mainly

concentrate between eta levels 0.745 and 0.59. Therefore, the structure of the NFSV-T and its corresponding energies indicate that the forecast accuracy of TC intensity measured by SLP is most sensitive to the uncertainties of the change in potential temperature that occurs between eta levels 0.745 and 0.59 (i.e., the middle and lower layers of the atmosphere) but around the TC center at the 24-h lead time.

The NFSV-Q structures are also shown to be independent of the TC cases and share a horizontal and vertical structure similar to NFSV-Ts, which for the TC case Dujuan is plotted in the second column in Fig. 2. It can be seen that positive moisture anomalies occur in the vertical layers from the surface to the middle troposphere and surround the TC center at the 24-h lead time, which, according to the definition, will be most likely to yield the largest deviation from the control forecast with respect to the SLP. In contrast to the NFSV-T, it is found that the majority of the energy of the NFSV-Q is concentrated within the middle layer of the atmosphere (i.e., the eta level from 0.71 to 0.59 in Fig. 3a), which accounts for 47.6% of the total energy of the NFSV-Q in the troposphere. This suggests that the uncertainty of moisture change in the mid-layer atmosphere plays a relatively more important role in the TC intensity forecast with a lead time of 24 h. Therefore, paying more attention to the simulation of moisture change in the mid-layer atmosphere and around the TC center at the 24-h lead time will be of benefit for a more accurate TC intensity forecast with the 24-h lead time.

When both the potential temperature and moisture tendency are simultaneously perturbed, the structures of the NFSV-TQs can be obtained for the nine TC cases and are also shown to be less case-dependent. The TC case Dujuan is still regarded as the example to describe the results (see the third column in Fig. 2). It is illustrated that the NFSV-TQs, as the optimal structure of the combined mode of potential temperature and moisture tendency perturbations, feature both NFSV-T and NFSV-Q, with positive anomalies occurring in both variables through the atmosphere in the vertical direction (except for negative anomalies of potential temperature at the surface) but only around the center of the TC at the 24-h lead time. However, we notice that the magnitudes of the moisture anomalies in the NFSV-TQ are much less than those of the NFSV-Q. Moreover, the internal energy component of the NFSV-TQ is larger than the moist energy component (see Fig. 3a). These findings suggest that the uncertainties of moisture change may play a secondary role in perturbing the SLP forecast, i.e., the accuracy of the TC intensity forecast with a lead time of 24 h may be more sensitive to the change of potential temperature than to that of moisture. Therefore, it is the change of the potential temperature, especially between the middle and lower layers of the atmosphere and around the TC center, that should be preferentially well-captured by the model to obtain a much more accurate TC intensity forecast.

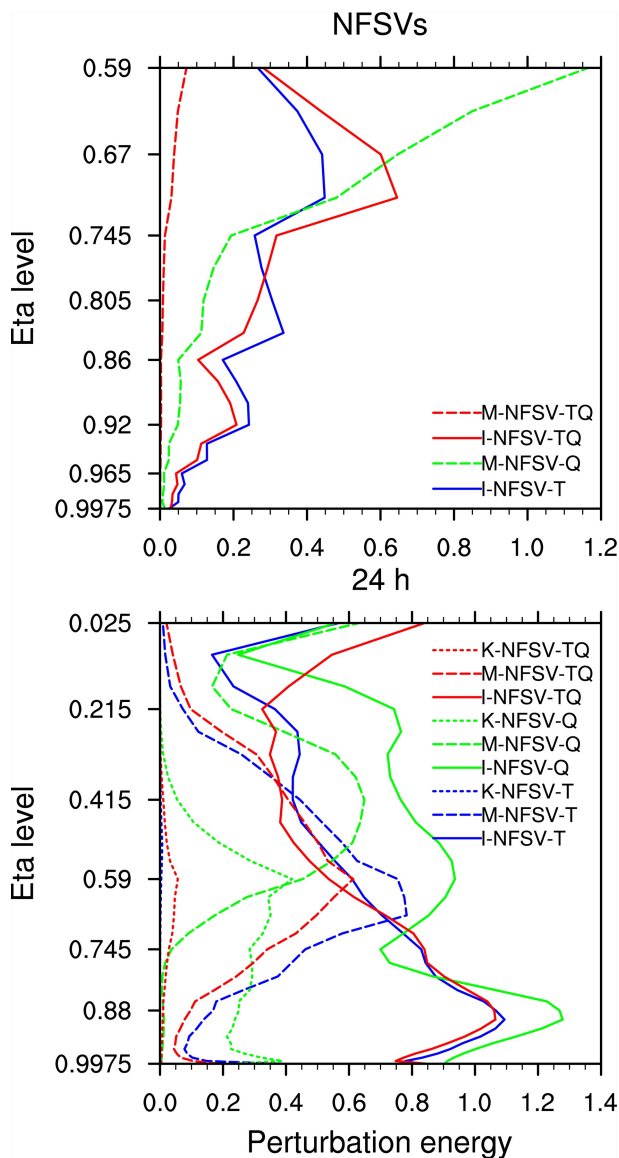


Fig. 3. Regionally averaged internal (I-), moist (M-), and kinetic (K-) energies (units: $10^{-2} \text{ J kg}^{-1}$) of NFSV-T (blue), NFSV-Q (green), and NFSV-TQ (red) (top), and their resultant energy deviation (units: 10^5 J kg^{-1}) (bottom) at the lead time of 24 h for the TC case Dujuan.

5. Impacts of NFSV-type tendency perturbations on TCs

NFSV-T, -Q, and -TQ are calculated based on the control forecast of TC intensity measured by the SLP. It is known with certainty that they will have the largest effect on the TC intensity forecast uncertainties. However, in the present study we are only concerned with the TC intensity forecast with a lead time of 24 h. From the traditional perspective, such short-range forecasts are more concerned with the accuracy of initial fields. Does it suggest that the NFSV-type tendency perturbation will not greatly change the control forecast during this 24 h? In addition, the MWS is also often used to describe the intensity of TCs. For the NFSV-type tendency perturbations predetermined by maximizing the minimum SLP, do they have a notable effect on the MWS of TCs? Moreover, we investigate in this section the impacts of the NFSV-tendency perturbations on the TC destructive force measured by the radial extent of gale force winds (GFWs), storm size and TC rainfall. Since similar results are obtained for the nine TC cases, we continue to use the TC case Dujuan as the example to illustrate the results.

5.1. TC Intensity

The minimum SLP of the TC case Dujuan without any perturbation (i.e., the control forecast; hereafter “CTRL”) is illustrated in Fig. 4. It can be seen that the minimum SLP slowly increases within the first 6 h (i.e., the time interval from -12 h to -6 h) and then experiences an abrupt drop by over 80 hPa during the time interval from -6 h to 0 h. From then (i.e., 0 h) on, the minimum SLP gradually increases and finally reaches approximately 1040 hPa at the 24-h lead time. Then, we superimpose the NFSV-tendency perturba-

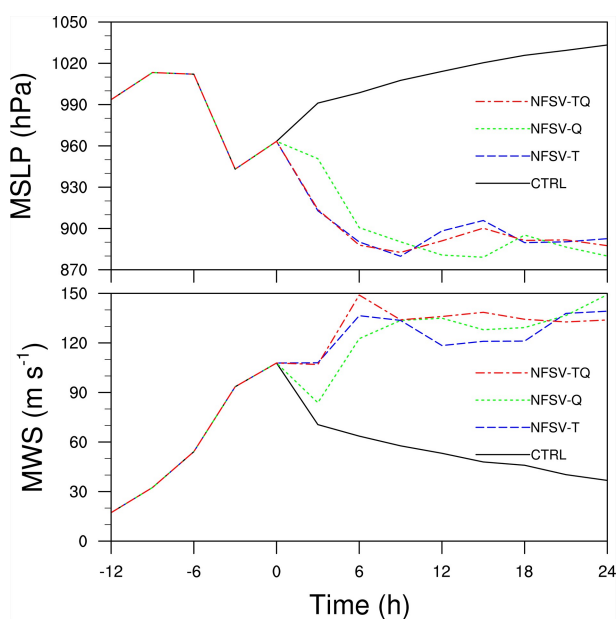


Fig. 4. Impacts of NFSV-T (blue), NFSV-Q (green), and NFSV-TQ (red) on the SLP (top) and MWS (bottom) for the TC case Dujuan, in contrast with CTRL (black).

tions on the CTRL during the time interval from 0 h to 24 h; that is, we produce a perturbed forecast of the SLP during the time interval from 0 h to 24 h with a start time of 0 h and a lead time of 24 h. When the NFSV-tendency perturbations are superimposed on the CTRL, it is apparent that the minimum SLPs begin to decrease and significantly depart from the CTRL. By calculation, a NFSV-T (NFSV-Q) magnitude of 10^{-4} K s^{-1} ($10^{-8} \text{ kg kg}^{-1} \text{ s}^{-1}$) can yield a significant forecast deviation from the CTRL in the minimum SLP of 140 hPa at the 24-h lead time. For all nine cases, NFSV-Ts (NFSV-Qs and NFSV-TQs) make the simulated storms stronger than the CTRL, some of which are even stronger than in reality, and with an average lower minimum SLP of 46.4 hPa (36.8 hPa and 52.7 hPa) than the best-track data. This indicates that even if a small perturbation to the change of potential temperature and/or moisture within the inner-core of TCs is superimposed, the forecast uncertainty of the SLP can quickly grow significantly, i.e., the NFSV-T, -Q, and -TQ can greatly change the TC intensity in the CTRL. Therefore, the accuracy of the TC intensity forecast with a short lead time of 24 h is very sensitive to the model errors represented by the tendency perturbation of the potential temperature and moisture of concern. Such sensitivity is partly due to the coarse resolution used and embodies the contribution of model errors in short-range TC intensity forecast uncertainty. It implies that a model with small model-error effect is necessary for the traditional perspective, which emphasizes the dominant contribution of initial accuracy to short-range forecasts of TC intensity.

The NFSV-T, -Q, and -TQ have considerable effects on the SLP in the CTRL. However, from Fig. 4 it can be seen that the NFSV-T takes a shorter time period than the NFSV-Q to make the minimum SLP the smallest, which suggests that the uncertainties of the potential temperature change rapidly decrease the subsequent SLP and then rapidly increase the TC intensity. This emphasizes that the change of TC intensity is more sensitive to the uncertainties of the change in potential temperature. In fact, when we investigate the optimal structure of the combined mode of potential temperature and moisture tendency perturbations in section 4, we find that the amplitude of the moisture component is much smaller than that of the potential temperature component and suggest that the uncertainties of the moisture change play a secondary role in perturbing the SLP forecast and emphasize the importance of potential temperature change in yielding uncertainties of SLP forecasts. It is obvious that the evolutionary behaviors of the differences between the CTRL and the forecasts disturbed by the NFSV-type tendency perturbations further verify the importance of the accuracy of potential temperature change in improving the TC intensity forecast skill.

The MWS is also often used to measure the TC intensity, and so we next investigate how the NFSV-type tendency perturbations derived by maximizing the minimum SLP affect the MWS of TCs. From Fig. 4, it is apparent that the MWS in the CTRL displays a rapid increase during the

time interval from -12 h to 0 h, which is followed by a slow decrease during the time interval from 0 h to 24 h. However, whenever the NFSV-tendency perturbations are imposed on the CTRL during the time interval from 0 h to 24 h, the MWS undergoes a significant change in terms of magnitude, which finally yields a deviation from the CTRL of ~ 100 m s^{-1} at the 24 -h lead time. This deviation is also reflected in the perturbation energies at the 24 -h lead time (see Fig. 3). Specifically, the large perturbation kinetics gather within the lower-layer atmosphere (i.e., below $\eta = 0.745$) and are obviously larger than both the inertial and moisture energies. As previously mentioned, the horizontal winds are not perturbed by the NFSV-tendency perturbations. Therefore, the large perturbation kinetics at the 24 -h lead time should be transferred from the inertial and/or moisture energy associated with the NFSV-T and -Q. In addition, it has been shown that the dominant inertial (and moisture) energies of NFSV-T (and NFSV-Q) are located within the mid- and low-layer (and mid-layer) atmosphere (see Fig. 3). Therefore, we infer that the large perturbation kinetic energy within the lower-layer atmosphere at the 24 -h lead time is partly transferred from the inertial and moisture energies in the mid-layer atmosphere. In other words, although the NFSV-type tendency perturbations are superimposed on the change of potential temperature and/or moisture and directly aimed at the forecast of the TC intensity measured by the minimum SLP, they can induce a well-developed storm system in the subsequent evolution of the TC. It is obvious that the small perturbations in the change of potential temperature and moisture can also induce significant forecast uncertainties of the MWS of the TC. Moreover, from Fig. 4 it can also be found that the MWS is more sensitive to the change of potential temperature than to that of moisture because the NFSV-Q spends a longer time period making the MWS the largest.

5.2. TC destructive force

As a criterion to issue TC-resultant gale warnings in operational forecasts, the radial extent of GFW is an important index to depict the TC destructive force, which is defined as the radial distance of the averaged tangential wind larger than 15.0 m s^{-1} from the TC center. The larger the radial extent, the larger the region that will be influenced by the gale. We compare the radial extent without and with NFSVs (figures omitted) and find that there is no region influenced by the gale from 9 h on in the CTRL of the TC case Dujuan; however, when the NFSV-tendency perturbations are superimposed on the CTRL, such a situation does not hold. With the NFSV-T perturbation, the GFW disappears earlier than that of the CTRL, whereas with the NFSV-Q perturbation the region influenced by the GFW becomes slightly larger. However, when the NFSV-TQ is superimposed on the CTRL, the GFW appears in the later times. We further explore the other eight cases and find that the NFSV-T, -Q, and -TQ perturbations influence the tangential wind in different ways. The NFSV-Q perturbation strengthens the tangential wind, rather than modulates the wind structure (also see

section 6). Therefore, the NFSV-Q perturbation can only lead to a larger radial extent of GFW than the CTRL. However, the NFSV-T perturbation tends to first change the wind structure but then gradually strengthens the tangential wind with time. Moreover, the change of wind structure does not make tangential wind larger during the forecast period but makes the region influenced by it more contracted than the CTRL due to the effect of the significantly strengthened near-surface radial winds. Moreover, we notice that the wind structure with the NFSV-TQ perturbation is similar to that of the NFSV-T, which suggests that the potential temperature change plays a dominant role in modulating the wind structure in TC intensity forecasts. Nonetheless, an accompanying effect on strengthening tangential wind induced by the moisture component in the NFSV-TQ makes the behavior of GFWs induced by the NFSV-TQ different from those caused by the NFSV-T and -Q.

The storm size, which is believed to impact surge, also indicates the destructive force of TCs. Next, we investigate the impact of the NFSVs on the storm size. In this study, the storm size is defined as the total number of grid points related to a storm where the surface wind speed is greater than a threshold. There are five grades of storm sizes in terms of surface wind speed: tropical storms (17.2 – 24.4 m s^{-1}), severe storms (24.5 – 32.6 m s^{-1}), typhoons (32.7 – 41.4 m s^{-1}), severe typhoons (41.5 – 50.9 m s^{-1}), and super typhoons (≥ 51 m s^{-1}). In Fig. 5, we plot their storm sizes for the TC case Dujuan at the lead times 6 h, 12 h, 18 h, and 24 h. It is shown that the region with large wind speed, particularly that of the severe typhoon for the CTRL, shrinks with time and disappears from 18 h on. Additionally, the wind speed in the right half of the TC is obviously larger than that in the left half from this time (i.e., 18 h), which appears to be an asymmetry of wind structure. These findings indicate that the TC case Dujuan is weakening in the CTRL. However, when it is disturbed by the NFSV-tendency perturbations (i.e., the NFSV-T, -Q, and -TQ), the storm sizes of the typhoon, severe typhoon, and super typhoon become significantly large, whereas the storm sizes of the tropical storm and severe storm expand significantly outward only when NFSV-T or NFSV-TQ is considered. That is, for the TC case Dujuan, not only does the wind speed in the inner-core become much larger, but more flows in the outer region are also involved. Even in cases such as Neoguri, Jangmi and Fungwong, the closed eyes in the CTRLs that disappear begin to reappear and even contract under the effect of the NFSVs, which indicates that the TCs are intensifying with the effect of the NFSVs. This implies that the uncertainties of the changes in both potential temperature and moisture can significantly influence the forecast uncertainty of the storm sizes. In particular, the change of the potential temperature significantly influences not only the wind speed in the inner core, but also the outer structure of TCs. Therefore, it tends to improve the ability to simulate the change in potential temperature and then increase the forecast skill of the storm size associated with the TC intensity.

TC rainfall is another important behavior of TC influ-

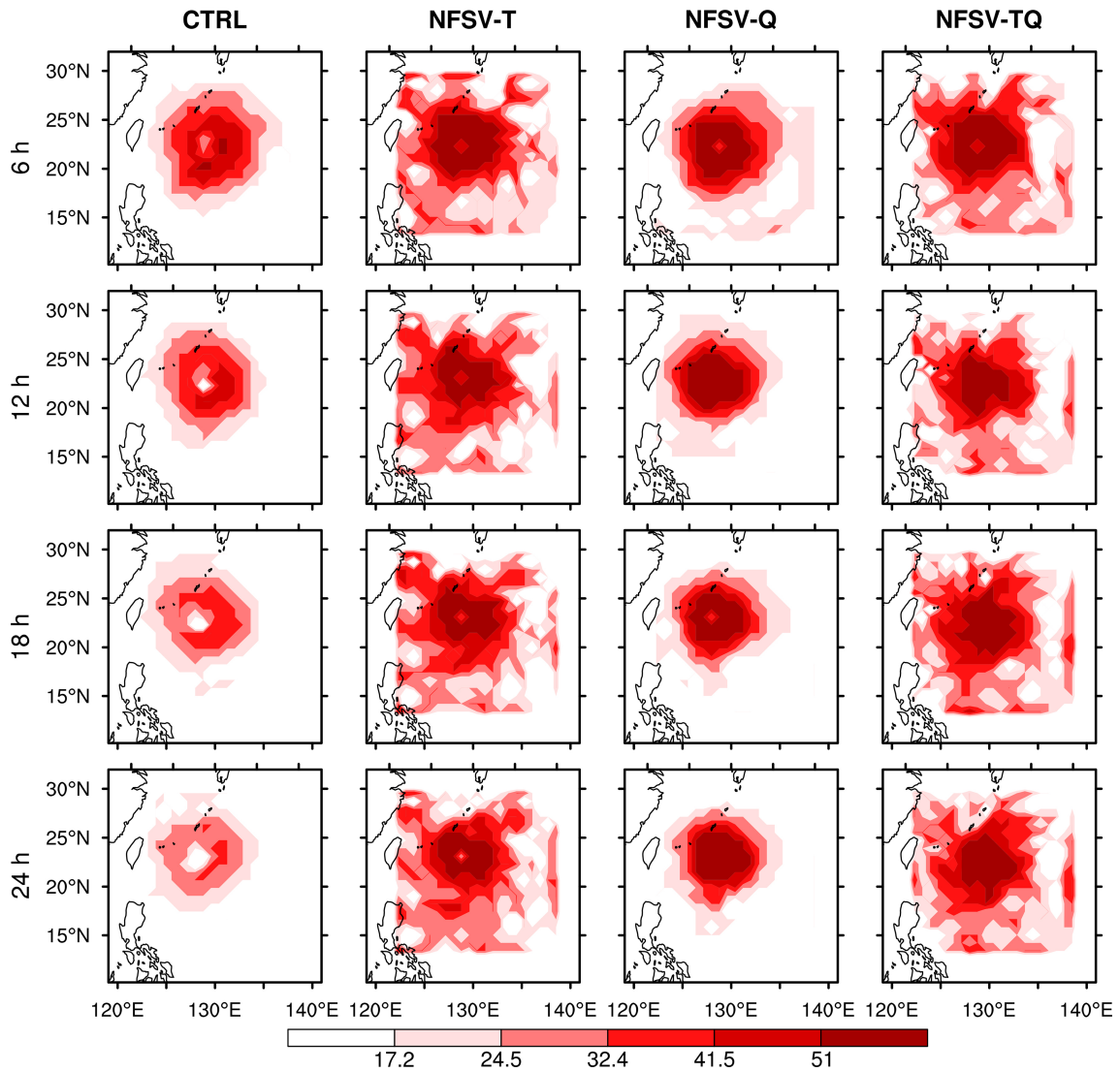


Fig. 5. Storm size in various grades according to the near-surface wind of CTRL, NFSV-T, NFSV-Q, and NFSV-TQ from 6 to 24 h at 6 h intervals, for the TC case Dujuan.

ence. The precipitation for the TC case Dujuan is concentrated between the period -12 h to -6 h (see Fig. 6), which dramatically decreases from then on; no measurable precipitation appears after 0 h in the CTRL. This situation remains the same when either NFSV-T or NFSV-TQ is added. However, if NFSV-Q is added, light rain appears from 0 h on and lasts to the end of the simulation. The distribution of perturbation energies gives a possible explanation for the different behaviors of NFSVs. For all NFSVs, only NFSV-Q leads to perturbation moist energy in the mid-layers of the atmosphere (Fig. 3). Neither NFSV-T nor NFSV-TQ can lead to significant differences for moisture at the 24-h lead time. Although there is a moisture component in NFSV-TQ, the amplitudes of the anomalies of the moisture component are much smaller than that of the potential temperature component. As a result, the impact of moisture change in NFSV-TQ is far away from measurable precipitation; only a sufficient change of moisture can lead to the obvious forecast differences for TC rainfall, which emphasizes the importance of ac-

curate simulation of the moisture change in precipitation forecasts.

6. Interpretation and verification

As demonstrated in section 5, the NFSV-tendency perturbations lead to large departures from the CTRL in terms of minimum SLP, MWS, the radial extent of GFW, storm size, and TC rainfall. In this section, we investigate their time-dependent evolution to study how the NFSV-tendency perturbations work and result in large departures from the CTRL. Subsequently, experiments are conducted to verify whether the ability to simulate SLP can be improved with the information provided by the sensitivity of NFSVs, especially for the WRF with a relatively coarse horizontal resolution as detailed in section 2. Since the conclusions are less case-dependent, we will still take the TC case Dujuan as the example to describe the results.

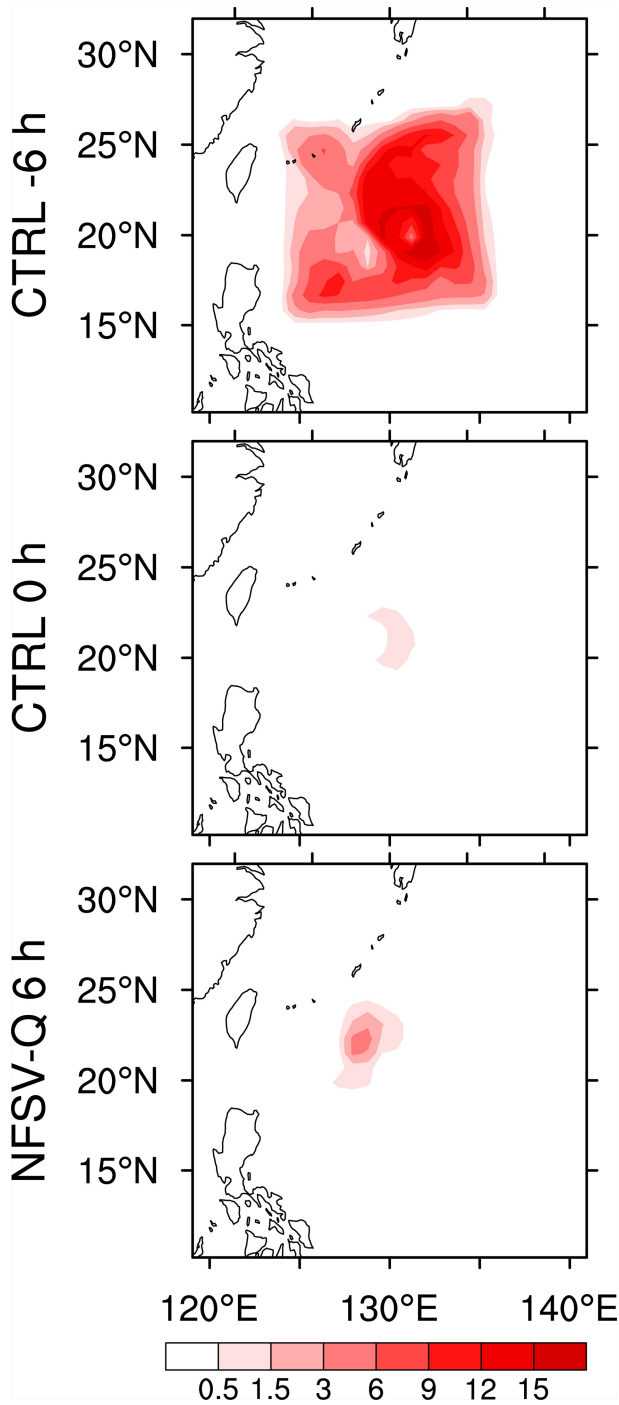


Fig. 6. TC rainfall (> 0.5 mm) at -6 h (top) and 0 h (center) in CTRL, and at 6 h in NFSV-Q (bottom) for the TC case Dujuan, respectively.

6.1. Pressure

The cost function to identify the NFSV-tendency perturbations is associated with the minimum SLP, which measures the TC intensity and is a function of pressure (see section 2). It is noted that the pressure is calculated by the equation of state $p = p_0(R_d\theta_m/p_0\alpha_d)^\gamma$, where p_0 , R_d , and γ are all constants and have values of 1000 hPa, 287.04 J kg $^{-1}$ K $^{-1}$, and 1.4, respectively. Obviously, the pressure p is deter-

mined by two variables: potential temperature (θ_m) and density of the dry air ($1/\alpha_d$). Since the NFSV-T represents the optimal tendency perturbation with respect to potential temperature, the NFSV-T directly leads to the change of pressure according to the equation of state. In the subsequent integration step, such change of pressure makes both the horizontal and vertical winds appear different from those of the CTRL; this process continues as NFSV-T is superimposed in each integration step. Simultaneously, the changed winds gradually induce intense secondary circulation and significantly decrease the density in the eye region, which further changes the pressure there. With the combined effects from both potential temperature and density, a large departure of SLP from the CTRL appears (as shown in Fig. 4). NFSV-Q works in a similar way, with the only difference that the change of moisture q_v is first transferred to that of potential temperature θ_m by $\theta_m = \theta[1 + (R_v/R_d)q_v] \approx \theta(1 + 1.61q_v)$. This gives a possible explanation that the change of moisture requires a longer time to reach the smallest SLP than potential temperature (as shown in Fig. 4), which further indicates the importance of accurate simulation to the change of potential temperature in improving the forecast skill for SLP.

6.2. Horizontal wind

Horizontal wind structure determines the MWS, the radial extent of GFW, and the storm size associated with TCs. We decompose the horizontal wind of the TC case Dujuan into radial and tangential components and plot them in Figs. 7 and 8, respectively, as a function of the radii from the TC center at various model eta levels at the lead times of 6 h, 12 h, 18 h, and 24 h. In contrast with that of the CTRL, both the radial and tangential winds, especially the former, with the NFSV-tendency perturbations at the near-surface (eta = 0.975 in Figs. 7 and 8), are stronger than the CTRL for most of the lead times, which directly contributes to the much larger MWSs in Fig. 4b and the expansion of storm sizes in typhoons, severe typhoons, and super typhoons in Fig. 5. Note that the location where the tangential wind reaches the maximum (which is larger than 15.0 m s $^{-1}$) determines the radial extent of the GFW. This location moves further away from the TC center (exceeding 540 km) when NFSV-Q is superimposed, whereas that for both NFSV-T and NFSV-TQ are only less than 540 km (as shown in Fig. 8). This is possibly why NFSV-Q behaves steadier in increasing the radial extent of GFW, as previously shown. Moreover, we notice that both the radial and tangential wind structures caused by NFSV-TQ are more similar to that of NFSV-T but are obviously different from that of NFSV-Q, which explains why the change of potential temperature plays the dominant role in disturbing the wind structure of TCs.

6.3. Precipitation

According to the distribution of TC rainfall in Fig. 6, we plot in Fig. 9 the relative humidity (RH) of the TC case Dujuan in the CTRL and that with the NFSV-tendency perturbations during the time intervals -6 h to 24 h, where the RH can determine if there is detectable precipitation. The

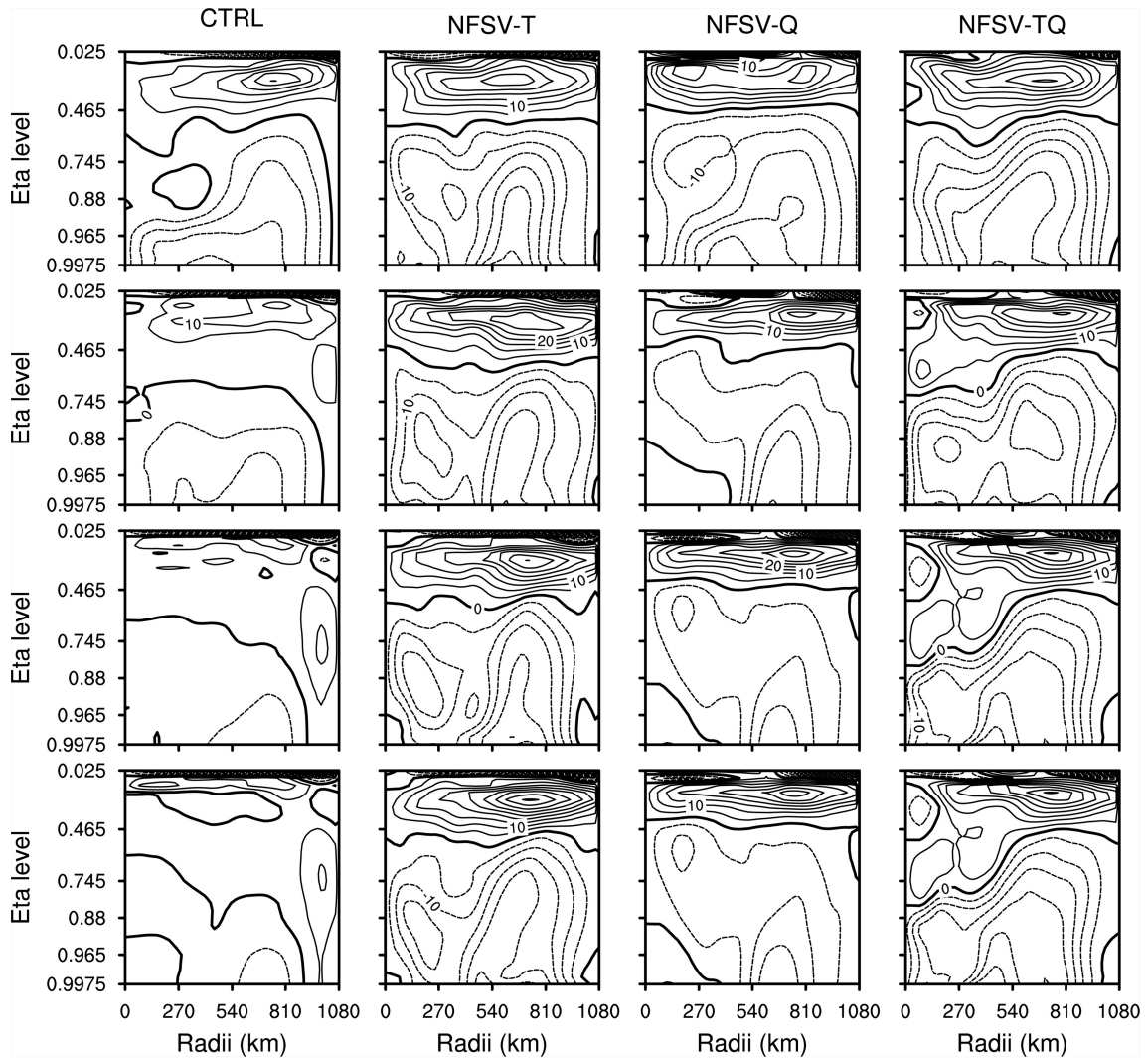


Fig. 7. Azimuthal-averaged radial wind (units: m s^{-1}) from the TC center to 1080 km in CTRL, NFSV-T, NFSV-Q, and NFSV-TQ for the TC case Dajuan.

RH at time -6 h is larger than 90% of that from the lower- (eta = 0.975) to the mid-layer (eta = 0.59) atmosphere (Fig. 9), which corresponds to heavy precipitation during this period (Fig. 6). In the subsequent 6 h (from -6 h to 0 h), the RH within this layer drops below 50%, which accords with light precipitation. When the NFSV-tendency perturbations are superimposed, only the NFSV-Q can lead to much larger RH than the CTRL within this layer. Moreover, the RH in the mid-layer atmosphere is obviously larger than that in the lower-layer atmosphere and is close to 100%. This possibly explains why precipitation only occurs when the NFSV-Q is superimposed on the CTRL.

6.4. Verification

Comparing Figs. 1 and 4, it is clear that the simulated minimum SLPs with the NFSV-tendency perturbations are significantly far away from the CTRL and close to the observed minimum SLPs. Furthermore, all of nine TC cases show such a phenomenon. This implies that the NFSV-type tendency perturbation may potentially describe model sys-

tem errors that limit the forecast skill of TC intensity. Additionally, the results in section 4 show that the NFSV-T sensitivity is more important for forecasting TC intensity and possesses a pattern with the main energies around the central location of the TCs at the 24-h lead time and located in the middle layers of the atmosphere. Such a pattern indicates that the model uncertainty that is represented by NFSV-T makes larger contributions to the forecast uncertainty of TC intensity. That is to say, the NFSV-T has more potential to describe the main model system error associated with forecasting TC intensity. In order to examine this possibility, we construct a correction item f_c to the tendency equation of potential temperature in WRF, derived as follows:

$$J(f_c) = \min_f [SLP_{t=T}(x_0, f) - MSLP]^2, \quad (4)$$

where $SLP_{t=T}(x_0, f)$ has a similar meaning as that in Eq. (2) and denotes the forecasted SLP at time T starting from the initial conditions x_0 with a correction item f ; whereas, MSLP denotes the minimum SLP of best-track data at the time T .

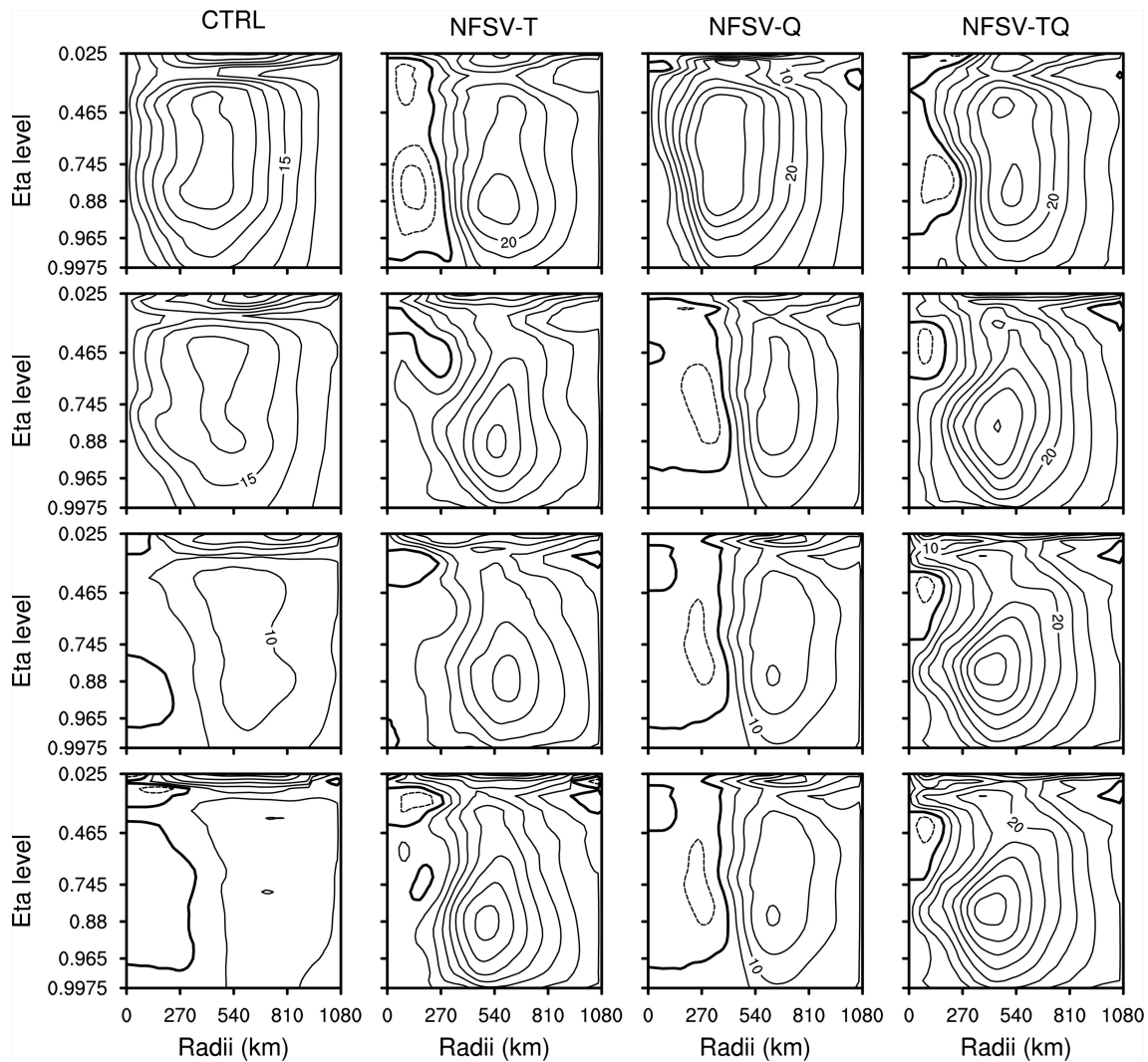


Fig. 8. As in Fig. 7 except for azimuthal-averaged tangential wind.

That is, Eq. (4) describes the minimum deviation of simulated minimum SLP with a correction item f_c from the best-track data. The smaller the minimum, the closer the simulated minimum SLP with f_c is to the observation. That is, the correction term f_c includes most of the information for correcting the CTRL. It is conceivable that, if the NFSV-T has the potential to describe the model system error of the TC intensity forecast, its pattern should bear useful information for the correction term f_c . To show this, we plot the simulated minimum SLP with the correction item f_c , together with the best-track data and the CTRL, for nine TC cases in Fig. 10 and the f_c . From Fig. 10, it is shown that, although there is a relatively large deviation from the best-track data at the lead time of 3 h, the simulated minimum SLPs with the correction item f_c are much closer to the best-track data during the following period than the CTRL; and the averaged deviation of minimum SLP with the correction item f_c from the best track is 4.5 hPa for nine TC cases, with the largest deviation of 14 hPa for the TC case Parma.

From Eq. (4), it is known that f_c mainly describes the model error effect of WRF with the 90-km horizontal resolu-

tion associated with TC intensity. When examining nine TC cases, we find that all f_c possess similar patterns. Therefore, f_c may reveal the model system error associated with the TC intensity. Figure 11 gives the f_c of the TC case Dujuan as an example. It is shown that the NFSV-T, either in its horizontal or vertical structures, is really similar to that of f_c . That is, the main energies are mainly around the central location of the TCs at the 24-h lead time and locate in the middle layers of the atmosphere. It is therefore inferred that the NFSV-T can describe the main model system error associated with the short-range forecast of TC intensity.

The NFSVs here are only related to the CTRL in its calculation and not as that in the calculation of the correction item f_c , which needs the future observation as the input (they cannot be available in forecasts). Furthermore, we have shown that the NFSV-T can describe the main model system errors of WRF associated with the short range of TC intensity. Therefore, we conceive that if calculating the NFSV-T with appropriate amplitudes (even together with the NFSV-Q) and superimposing them to the tendency of WRF, the short-range forecast skill of TC intensity could be

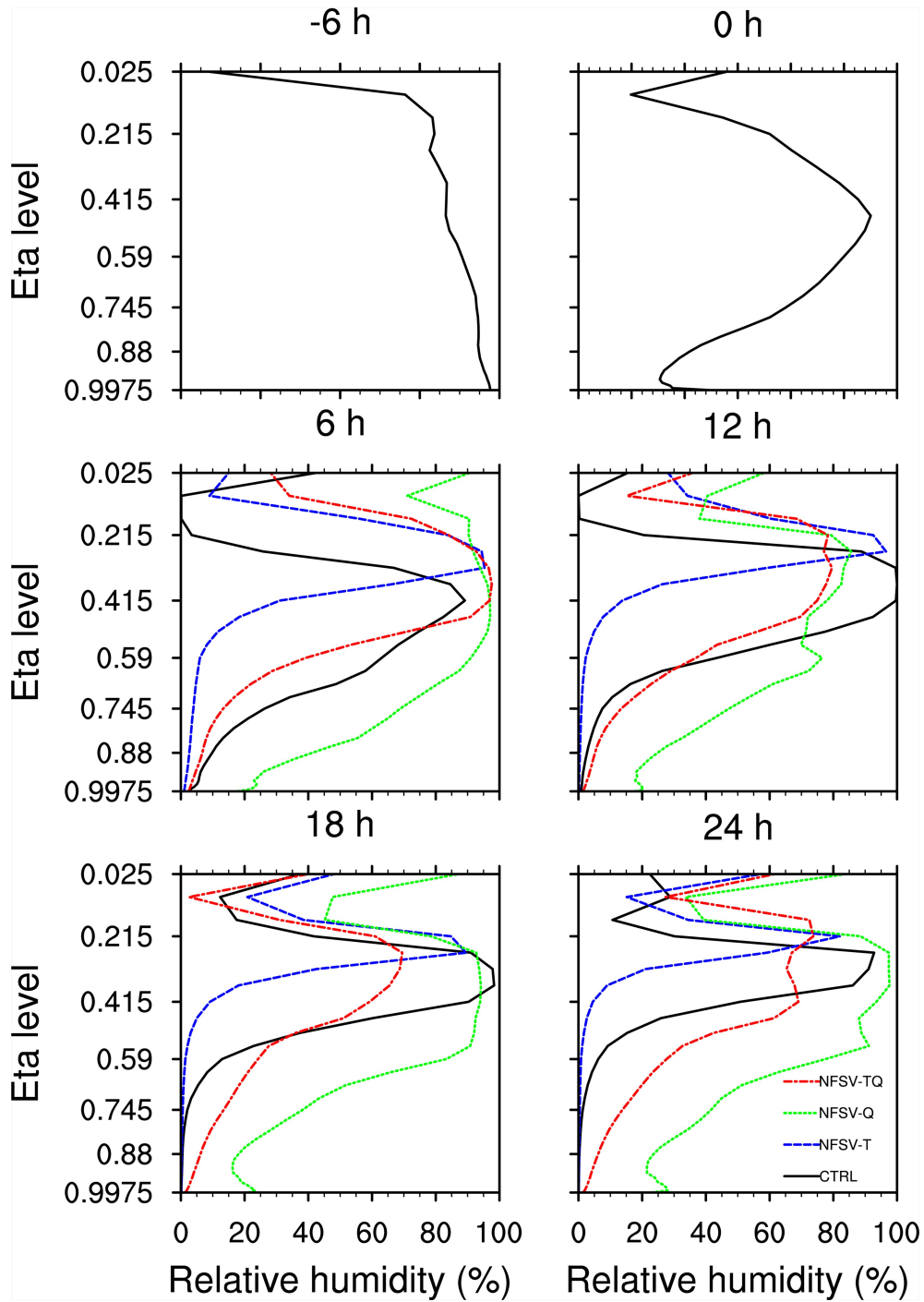


Fig. 9. Regionally averaged RH in CTRL (black), NFSV-T (blue), NFSV-Q (green), and NFSV-TQ (red) from -6 h to 24 h at every 6 h interval for the TC case Dujuan.

greatly improved, especially for models with coarse resolution and being unable to precisely resolve small-scale dynamic processes but being expected to be used for TC intensity forecasts. Of course, one can also consider regarding the NFSVs as members of ensemble forecasts for TC intensity and increase the ensemble spread as shown in some other ensemble forecast methods (see Introduction). In any case, it is expected that the NFSV approach can play a role in improving the TC intensity forecast skill.

7. Summary and discussion

In this study, we use the NFSV approach to identify the tendency perturbations of the WRF model that will lead to the largest deviation of the minimum SLP from the control forecast at the 24-h lead time. The optimal tendency perturbations of potential temperature, moisture and their combined mode, denoted by “NFSV-T”, “NFSV-Q”, and “NFSV-TQ”, respectively, are revealed for nine selected TC cases.

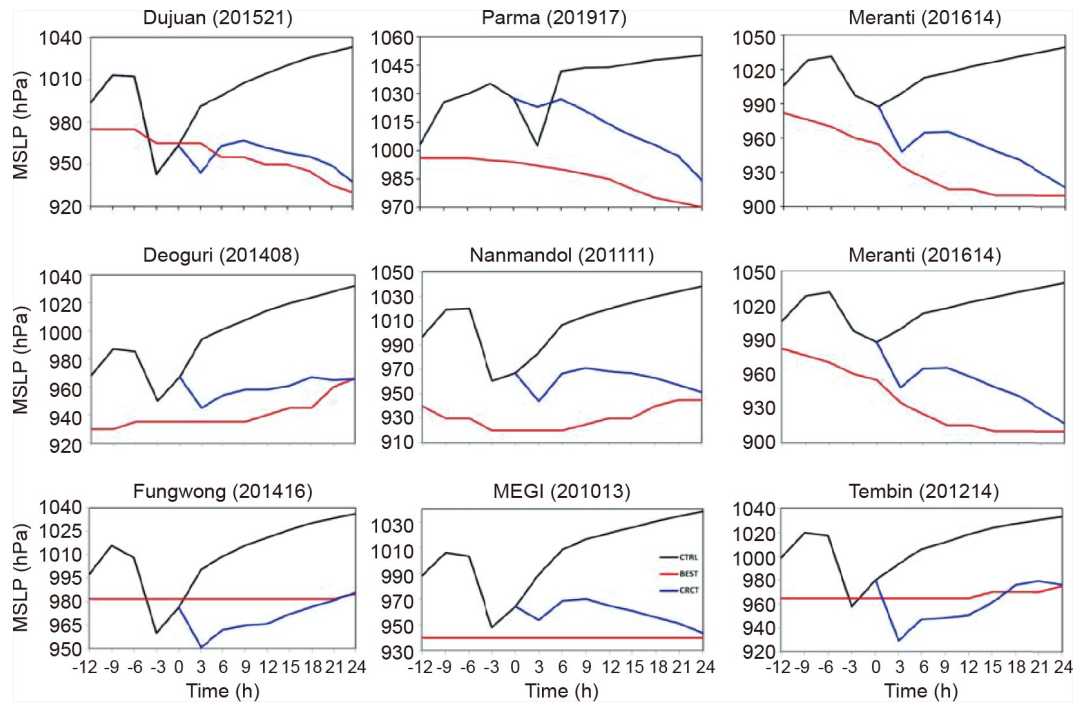


Fig. 10. The SLP in best-track data (red), CTRL (black), and with the correction item (blue) for nine TC cases.

All of these NFSV-tendency perturbations are shown to have a coherent barotropic structure with height, and their dominant energies are concentrated around the center of the TC at the 24-h lead time but are only located in the mid-layer or mid- and lower-layer atmosphere. Moreover, such tendency perturbation structures do not depend on TC intensities and what the TC undergoes in the following stage. The NFSV-tendency perturbations for TCs indicate that the forecast accuracy of TC intensity measured by SLP are more sensitive to the uncertainties of the changes of the potential temperature (moisture) that occur in the mid- and lower-layer (mid-layer) atmosphere but in the inner-core of TCs at the 24-h lead time. A comparison was made between the potential temperature and moisture, and the uncertainties of the potential temperature change are shown to play a more important role in disturbing the forecast accuracy of the minimum SLP, and even the MWS, the radial extent of GFW, and the storm size. The forecast skill of TC intensity can therefore benefit more from the accuracy of the potential temperature change, especially in the region between the mid- and lower-layer atmosphere but also in the inner-core of TCs. However, for TC rainfall, the moisture change accuracy is found to be more crucial to the improvement of TC rainfall forecast skill.

It is noted that the TC intensity forecasts with 24-h lead time are of concern. From the traditional perspective, such short-range forecasts are more concerned with the accuracy of initial fields. However, this does not mean that the uncertainty coming from an imperfect model can be ignored. Conversely, the present study shows that even if a tiny tendency perturbation is superimposed on potential temperature and/or moisture, an aggressively large departure from the con-

trol forecast of the SLP can result, even within a short-range forecast such as a lead time of 24 h. Moreover, additional experiments (details not shown here) suggest that the TC intensity (indicated by the minimum SLP) will quickly approach that of the control when the NFSV-T, -Q, or -TQ are removed at any time during the 24-h lead time, which in fact emphasizes the importance of model uncertainty in disturbing the accuracy of TC intensity forecasts. Obviously, this is quite different from the traditional perspective and is probably related to the model uncertainty itself because a WRF with coarse resolution is used. Despite this, the results provide useful ideas on improving TC intensity forecast skill, even with a WRF of coarse resolution. Specifically, according to the structure of the NFSV-tendency perturbations shown in the present study, we have indicated that the forecast of TC intensity measured by minimum SLP is more sensitive to the uncertainty in the change of potential temperature in the inner core of a TC. Hence, we construct an optimal correction item to force the simulated minimum SLP at a lead time of 24 h to approach the best-track data, and such a correction item describes model system errors associated with TC intensity simulation. In particular, the present study has found that the NFSV-T bears great similarities with this correction term and its resultant TC intensity forecast is close to the best-track data. Obviously, the NFSV-T possess more potential to offset the model system error effect and improve the TC intensity forecast skill. In the present study, WRF with a horizontal resolution of 90 km is adopted. It is therefore conceivable that the TC intensity forecast, even if the adopted model has an insufficiently fine resolution to resolve the small-scale dynamics, also has the potential to achieve high skill due to the inclusion of NFSV sensit-

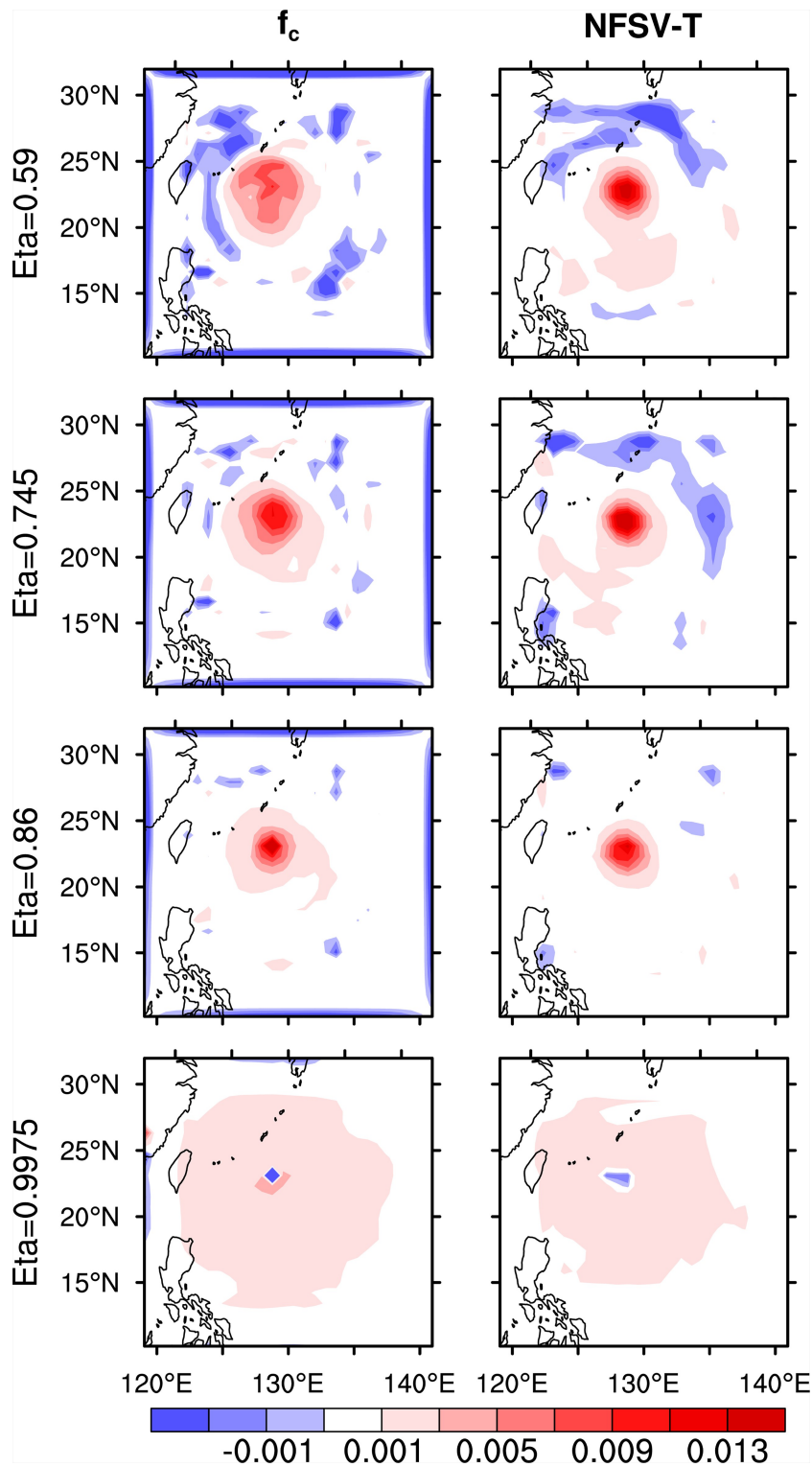


Fig. 11. The f_c (left; units: 10^{-1} K s^{-1}) and NFSV-T (right; units: K s^{-1}) for the TC case Dujuan at different eta levels.

ivity.

In addition, Emanuel and Zhang (2017), from the perspective of initial value problems, stated that the growth of TC intensity forecast errors are at least as sensitive to the specification of inner-core moisture as to that of the wind field. In the present study, from a perspective of tendency perturba-

tion, the TC intensity forecast is shown to be more sensitive to the change of potential temperature than to that of moisture. Which one, then, between the initial condition of moisture and change of potential temperature, is more important for TC intensity forecasts? And what about the sensitivity of initial potential temperature? These questions should be ex-

plored in the future. The answers will be helpful for addressing whether the initial field or model accuracy should be of greater concern, and which physical variable in which region should be of greater concern in improving accuracy and significantly increasing the forecast skill of TC intensity. In any case, we expect that the TC intensity forecast can be made more skillful through more studies on the predictability of TCs.

Acknowledgements. The authors appreciate the two anonymous reviewers very much for their insightful comments and suggestions. This work was jointly sponsored by the National Key Research and Development Program of China (Grant No. 2018YFC1506402) and the National Natural Science Foundation of China (Grant Nos. 41930971, 41575061 and 41775061).

REFERENCES

- Barkmeijer, J., T. Iversen, and T. N. Palmer, 2003: Forcing singular vectors and other sensitive model structures. *Quart. J. Roy. Meteorol. Soc.*, **129**, 2401–2423, <https://doi.org/10.1256/qj.02.126>.
- Berner, J., G. J. Shutts, M. Leutbecher, and T. N. Palmer, 2009: A spectral stochastic kinetic energy backscatter scheme and its impact on flow-dependent predictability in the ECMWF ensemble prediction system. *J. Atmos. Sci.*, **66**, 603–626, <https://doi.org/10.1175/2008JAS2677.1>.
- Bhatia, K. T., D. S. Nolan, A. B. Schumacher, and M. DeMaria, 2017: Improving tropical cyclone intensity forecasts with PRIME. *Wea. Forecasting*, **32**, 1353–1377, <https://doi.org/10.1175/WAF-D-17-0009.1>.
- Birgin, E. C., J. Mario, Martinez, and M. Raydan, 2001: Algorithm 813: SPG-software for convex-constrained optimization. *ACM Transactions on Mathematical Software*, **27**, 340–349, <https://doi.org/10.1145/502800.502803>.
- Buizza, R., M. Milleer, and T. N. Palmer, 1999: Stochastic representation of model uncertainties in the ECMWF ensemble prediction system. *Quart. J. Roy. Meteorol. Soc.*, **125**, 2887–2908, <https://doi.org/10.1002/qj.49712556006>.
- DeMaria, M., C. R. Sampson, J. A. Knaff, and K. D. Musgrave, 2014: Is tropical cyclone intensity guidance improving? *Bull. Amer. Meteorol. Soc.*, **95**, 387–398, <https://doi.org/10.1175/BAMS-D-12-00240.1>.
- Duan, Q. S., and P. Zhao, 2015: Revealing the most disturbing tendency error of Zebiak-Cane model associated with El Niño predictions by nonlinear forcing singular vector approach. *Climate Dyn.*, **44**, 2351–2367, <https://doi.org/10.1007/s00382-014-2369-0>.
- Duan, W. S., and F. F. Zhou, 2013: Non-linear forcing singular vector of a two-dimensional quasi-geostrophic model. *Tellus A: Dynamic Meteorology and Oceanography*, **65**, 18452, <https://doi.org/10.3402/tellusa.v65i0.18452>.
- Duan, W. S., B. Tian, and H. Xu, 2014: Simulations of two types of El Niño events by an optimal forcing vector approach. *Climate Dyn.*, **43**, 1677–1692, <https://doi.org/10.1007/s00382-013-1993-4>.
- Ehrendorfer, M., R. M. Errico, and K. D. Raeder., 1999: Singular-vector perturbation growth in a primitive equation model with moist physics. *J. Atmos. Sci.*, **56**, 1627–1648, [https://doi.org/10.1175/1520-0469\(1999\)056<1627:SVP-GIA>2.0.CO;2](https://doi.org/10.1175/1520-0469(1999)056<1627:SVP-GIA>2.0.CO;2).
- Emanuel, K., and F. Q. Zhang, 2016: On the predictability and error sources of tropical cyclone intensity forecasts. *J. Atmos. Sci.*, **73**, 3739–3747, <https://doi.org/10.1175/JAS-D-16-0100.1>.
- Emanuel, K., and F. Q. Zhang, 2017: The role of inner-core moisture in tropical cyclone predictability and practical forecast skill. *J. Atmos. Sci.*, **74**, 2315–2324, <https://doi.org/10.1175/JAS-D-17-0008.1>.
- Gentry, M. S., and G. M. Lackmann, 2010: Sensitivity of simulated tropical cyclone structure and intensity to horizontal resolution. *Mon. Wea. Rev.*, **138**, 688–704, <https://doi.org/10.1175/2009MWR2976.1>.
- Green, B. W., and F. Q. Zhang, 2013: Impacts of air-sea flux parameterizations on the intensity and structure of tropical cyclones. *Mon. Wea. Rev.*, **141**, 2303–2324, <https://doi.org/10.1175/MWR-D-12-00274.1>.
- Huo, Z. H., 2016: The application of nonlinear optimal perturbations methods in ensemble forecasting. PhD dissertation, University of Chinese Academy of Sciences, 108 pp. (in Chinese)
- Judt, F., S. S. Chen, and J. Berner, 2016: Predictability of tropical cyclone intensity: Scale-dependent forecast error growth in high-resolution stochastic kinetic-energy backscatter ensembles. *Quart. J. Roy. Meteorol. Soc.*, **142**, 43–57, <https://doi.org/10.1002/qj.2626>.
- Lang, S. T. K., M. Leutbecher, and S. C. Jones, 2012: Impact of perturbation methods in the ECMWF ensemble prediction system on tropical cyclone forecasts. *Quart. J. Roy. Meteorol. Soc.*, **138**, 2030–2046, <https://doi.org/10.1002/qj.1942>.
- Leutbecher, M., and Coauthors, 2017: Stochastic representations of model uncertainties at ECMWF: State of the art and future vision. *Quart. J. Roy. Meteorol. Soc.*, **143**, 2315–2339, <https://doi.org/10.1002/qj.3094>.
- Ollinaho, P., and Coauthors, 2017: Towards process-level representation of model uncertainties: Stochastically perturbed parameterizations in the ECMWF ensemble. *Quart. J. Roy. Meteorol. Soc.*, **143**, 408–422, <https://doi.org/10.1002/qj.2931>.
- Palmer, T. N., R. Buizza, F. Doblas-Reyes, T. Jung, M. Leutbecher, G. J. Shutts, M. Steinheimer, and A. Weisheimer, 2009: Stochastic parametrization and model uncertainty. Technical Memorandum 598.
- Puri, K., J. Barkmeijer, and T. N. Palmer, 2001: Ensemble prediction of tropical cyclones using targeted diabatic singular vectors. *Quart. J. Roy. Meteorol. Soc.*, **127**, 709–731, <https://doi.org/10.1002/qj.49712757222>.
- Reynolds, C. A., J. G. McLay, S. J. Goerss, E. A. Serra, D. Hodys, and C. R. Sampson, 2011: Impact of resolution and design on the U. S. Navy global ensemble performance in the Tropics. *Mon. Wea. Rev.*, **139**, 2145–2155, <https://doi.org/10.1175/2011MWR3546.1>.
- Sippel, J. A., and F. Q. Zhang, 2010: Factors affecting the predictability of Hurricane Humberto (2007). *J. Atmos. Sci.*, **67**, 1759–1778, <https://doi.org/10.1175/2010JAS3172.1>.
- Torn, R. D., 2016: Evaluation of atmosphere and ocean initial condition uncertainty and stochastic exchange coefficients on ensemble tropical cyclone intensity forecasts. *Mon. Wea. Rev.*, **144**, 3487–3506, <https://doi.org/10.1175/MWR-D-16-0108.1>.
- Zou, X., F. Vandenberghe, M. Pondecà, and Y. H. Kuo, 1997: Introduction to Adjoint techniques and the MM5 Adjoint Modeling System. NCAR Technical Note, NCAR/TN-435-STR, 111 pp.